Hindawi
Advances in Civil Engineering
Volume 2019, Article ID 2586242, 12 pages
https://doi.org/10.1155/2019/2586242

Research Article

Wind Tunnel Test Investigation on Unsteady Aerodynamic Coefficients of Iced 4-Bundle Conductors

Mengqi Cai,[1] **Linshu Zhou**,[2] **Hang Lei**,[3] **and Hanjie Huang**[4]

[1]*School of Civil Engineering & Architecture, Chengdu University, Chengdu 610106, China*
[2]*State Grid Sichuan Integrated Energy Service Co. LTD, Chengdu 610072, China*
[3]*School of Naval Architecture, Ocean & Civil Engineering, Shanghai Jiaotong University, Shanghai 200240, China*
[4]*China Aerodynamics Research and Development Center, Mianyang 621000, China*

Correspondence should be addressed to Hanjie Huang; hansjie@hotmail.com

Received 16 December 2018; Revised 29 April 2019; Accepted 23 May 2019; Published 13 June 2019

Academic Editor: Stefano de Miranda

Iced conductor motion is induced by the aerodynamic instability of these conductors. The unsteady aerodynamic characteristics are different from the steady aerodynamic characteristics. The unsteady aerodynamic coefficients of typical iced conductors' models under torsional motion are measured by the unsteady wind tunnel test. The unsteady aerodynamic coefficients of crescent-shape and sector-shape iced 4-bundle conductors under different torsional motion frequencies, wind velocities, and ice thicknesses are obtained. Wind test results show that there are significant differences between the unsteady and steady aerodynamic coefficients. The unsteady aerodynamic coefficients curve is a loop which is different from the steady aerodynamic coefficients. In addition, the obvious differences exist between unsteady aerodynamic coefficients of crescent-shape and sector-shape iced bundle conductors. Critical parameters, including torsional motion frequencies, wind velocity, ice shape, and ice thickness, have significant influences on unsteady aerodynamic coefficients. It shows that the wind tunnel experiment results are able to provide necessary data for the investigation of iced bundle conductor motion and their prevention techniques.

1. Introduction

4-bundle conductor 500 kV ultra-high voltage (UHV) transmission lines have been widely launched to solve the imbalance problem between electric power supply and demand. Because of the complexity and instability of natural environment, the safe operation of iced transmission lines has attracted wide attention when the conductors are covered with heavy ice [1, 2]. Transmission lines may be subjected to iced conductor motion in the forms of galloping, wake-induced oscillation, and ice jump [3]. Iced conductor motion may lead to short circuit hardware failure, conductor's failure, and even collapse of towers, which usually leads to power interruption. Thus, the control of iced conductor motion is still a hot topic in electrical engineering. The iced conductor motion of bundle conductor transmission lines is a typical fluid structure interaction (FSI) motion [4]. These motions are induced by the aerodynamic instability of conductors. However, lack of profound understanding of iced conductor motion response has frustrated the improvement of anticonductor motion techniques.The ice accumulated on the bundle conductors is noncircular due to its large torsional stiffness; thus, it occurs more common on the bundle conductors than on a single conductor [5]. Therefore, it is necessary to investigate the aerodynamic forces of the bundle conductors in UHV transmission lines, especially the heavy iced 4-bundle conductors in cold regions.

The aerodynamic characteristics should be determined firstly, in order to investigate iced conductor motion behaviors of iced bundle transmission lines [3]. The aerodynamic coefficients of different types of iced conductor models were measured and anglicized in the research of Hartog [4]. They pointed out that the aerodynamic coefficients determined by the quasisteady wind tunnel test

appear to be reasonable descriptions of the conductor motion phenomena in uniform and turbulent flows. Numerical models for motion analysis of subconductors rely on quasisteady theory (QST) [5–10]. Then, the torsional motion mechanism and the protective measures of galloping were proposed by Nigol et al. [11–13] through the experimental investigation of these iced single conductors. Chabart and Lilien [14] measured the steady aerodynamic characteristics of a series of single conductors by using the wind tunnel test. These test studies focused on the steady aerodynamic coefficients of single conductors.

To investigate the effects of the air flow on the bundle conductors, Wardlaw and Cooper [15] conducted wind tunnel test to investigate the steady aerodynamic forces on 2-bundle conductors. The steady aerodynamic coefficients of crescent-shape iced 4-bundle conductors varying with wind attack angle measured by wind tunnel tests were presented by Hu et al. [16]. In addition, in the finite element method (FEM) ABAQUS software, the cable elements were created by the releasing of the bending degree-of-freedom of Euler beam element. The galloping behaviors of iced 4-bundle conductors under different working conditions were numerically simulated. Then, the effects of wake interference around these subconductors on transmission lines motion characteristics were discussed. Xie et al. [17] implemented a series of wind tunnel experiments to obtain the steady drag coefficients (same as wind pressure coefficients) of the bundle conductors to investigate the differences between global drag coefficients of bundle conductors and single conductor. Diana et al. [18] implemented a wind tunnel experiment to acquire the steady aerodynamic coefficients of the 4-bundle conductors. The experiment test concluded that the effect of air flow interference around subconductors cannot be ignored. Yan et al. [19] used wind tunnel test to measure the aerodynamic coefficients of 4-bundle conductors; the aerodynamic coefficients of each subconductor varying with wind attack angles were obtained. Yan et al. [20] proposed the numerical method to investigate galloping behaviors of iced 4-bundle conductor lines based on the results of crescent-shape iced 4-bundle conductors obtained by the wind tunnel test. Wind tunnel tests were carried out by Li et al. [21] to obtain the steady aerodynamic characteristics of crescent-shape iced 4-bundle conductors which are used in 500 kV UHV transmission lines with different test conditions (ice thicknesses, initial ice accretion angles, bundle spaces, and wind attack angles). Wind tunnel tests were carried out by Lou et al. [22] to acquire the steady aerodynamic characteristics of iced 6-bundle conductors in different analysis parameters which are used in 750 kV UHV transmission lines. Similar conclusions have been obtained by Zhou et al. [23]; the steady aerodynamic coefficients of crescent-shape iced 8-bundle conductors were obtained by the wind tunnel test. The test models with a real rough surface were made of the actual conductors. Cai et al. [24] used FEM ABAQUS software to validate the availability of the aerodynamic coefficients determined by computational fluid dynamics (CFD) in the analysis of galloping characteristics of iced 4-bundle conductors and compared numerical results with the steady aerodynamic coefficients of these iced 4-bundle conductors acquired by wind tunnel measurements. Wu et al. [25] used CFD FLUENT software to obtain the aerodynamic coefficients of 2-bundle conductors with conceding the different conductor space.

These studies mentioned above are all based on quasisteady theory. The steady aerodynamic coefficients are obtained from the wind tunnel experiments. Investigation on the unsteady aerodynamic loads of iced bundle conductors is still lacking, so it is urgent to obtain the unsteady aerodynamic loads of each subconductor of iced bundle conductors. Meanwhile, the above studies focused on the bare bundle conductors or crescent-shape and D-shape iced bundle conductors; the investigations on aerodynamic coefficients of sector-shape iced bundle conductors are also less reported.

Here, the unsteady aerodynamic behaviors of crescent-shape and sector-shape iced 4-bundle conductors are firstly acquired by wind tunnel measurements, in order to study the unsteady aerodynamic coefficients of 4-bundle 500 kV transmission lines. Tests are put into effect to acquire the unsteady aerodynamic characteristics of iced 4-bundle conductors varying with the wind attack angles under different torsional motion frequencies, ice shape, wind velocities, and ice thicknesses in the wind tunnel. The obtained results may provide the fundamental data for the development of antimotion techniques of 4-bundled conductor transmission lines.

2. Wind Tunnel Measurements for the Unsteady Aerodynamic Coefficients

2.1. Test Model. The aerodynamic forces of bundle conductors are the foundations of analysis of the conductor motion of transmission lines [5]. The aerodynamic loads acted on the 4-bundle conductors are obtained by experiments. The distance between two adjacent subconductors (D) is 450 mm. The length, L, of the conductor model is 710 mm. The material of ice model is wood and the length of test model is 710 mm. The outside layer of conductor model has been put on some rubber tubes to simulate the surface of real conductor.

Hard ice and glaze deposits are tough enough; they have enough elasticity and strength so that they cannot be moved away. Wind-driven wet snow may accumulate gradually on the windward sides of subconductors, which cause a hard and sharp leading edge. These formed ice shapes may lead to conductor motion. Combined with actual observation, crescent-shape and sector-shape can be generalized with respect to the great variety of natural heavy ice shape [16, 20]. The aerodynamic forces of bundle conductors are the foundations of analysis of the conductor motion of transmission lines [5]. Here, the unsteady aerodynamic coefficients of crescent-shape and sector-shape iced 4-bundle conductors are obtained by experiments. The cross section of iced models is shown in Figure 1. The arc angle of sector-shape ice type is 120° (Figure 1(b)).

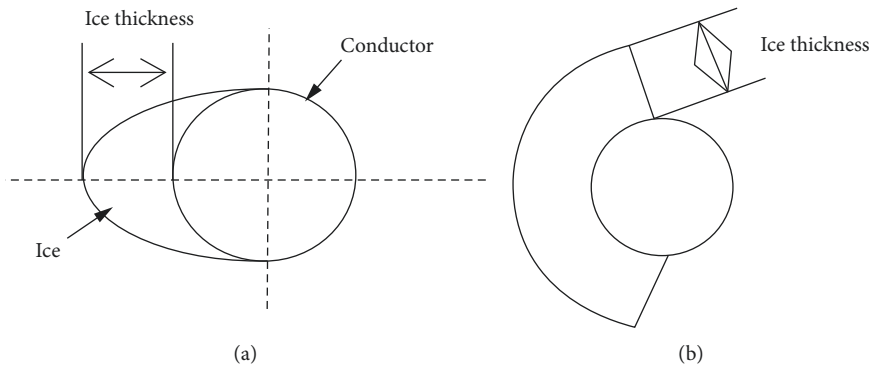

Figure 1: Cross section of iced model: (a) crescent and (b) sector.

The ice and conductor models are displayed in Figure 2. The stranded surface conductor model (4×LGJ-400/50) is shown in Figure 2(a), which is close to the real conductor. The diameter (d) of each subconductor is 27.63 mm. The diameter ratio of the real conductor model to the test model is 1 : 1. The artificial crescent-shape and sector-shape ice model with different ice thickness is made of light wood with density close to the density of the real ice (836.81 kg/m^3), and the ice is shown in Figure 2(b). The ice thickness of crescent-shape ice type is set as 14.5 mm, 24 mm, and 33 mm, respectively. The ice thickness of sector-shape ice type is set as 21.5 mm and 30 mm, respectively. As shown in Figure 2, these studies are closer to the real situation than the smooth surface cylinder and those artificial with rubber tubes used in most literature experiments. The ice type is fixed on the surface of the conductor model.

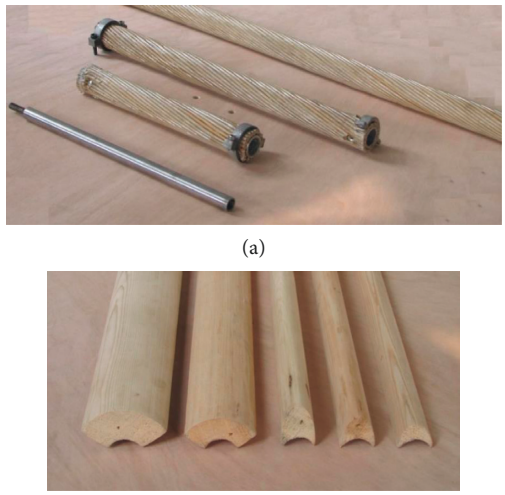

Figure 2: The test model of conductor: (a) conductor model and (b) ice model.

2.2. Wind Tunnel. As shown in Figure 3(a), the conductor models are installed vertical between two circular plates which can keep two-dimensional characteristics of the inflow. The tests of the sectional 4-bundle conductors are arranged in the wind tunnel (1.4 m × 1.4 m) (Figure 3). The crescent-shape iced and sector-shape iced 4-bundle conductors in wind tunnel are listed in Figures 3(a) and 3(b).

The length of test section is 2.8 m (Figure 4(a)), the conductor model is in the middle of wind tunnel, and the range of wind velocity is 0 m/s~65 m/s. Observation of transmission lines galloping shows that iced conductor motion occurs in the wind velocity (from 4 m/s to 20 m/s) in most cases. In Figure 4(b), the wind attack angle (α) is defined. The initial wind attack angle is 0°, based on the test of Nigol and the filed survey. The aerodynamic forces at all subconductors are measured under different wind attack angles in the range from −45° to 45°, with an increment of 0.5° (considering the cost and accuracy of wind tunnel test, the increment is set to be 0.5°). All aerodynamic forces are in wind coordinate system. The Symbols and abbreviations are listed in Table 1.

As shown in Figure 5, the TG0151 rod-type balance is installed inside the conductor model. The conductor models and balance are linked by connecting pieces, which are fixed in the middle position of the conductor model (Figure 5(a)). The upper side of the balance is arranged on the steel brackets, which is fixed on the rigid frame of the special supporting device for the conductor model. The steel bracket has a groove to accommodate the balance signal line. The conductor model is mounted vertically on a special supporting device located at the center of the turntable in the wind tunnel test section. The special supporting device is divided into three parts: the base, the rotating shaft (drive motor), and the fixing frame (Figure 5(b)). The drive motor is made of steel, covered with a circular upper end plate. The turntable and the fixing frame are directly fixed and connected with the base through bearings.

The aerodynamic coefficients of 4-bundle conductors (i.e., the drag coefficients, lift coefficients, and torsional moment coefficients) are measured by TG0151 balance. The TG0151 balance is applied to measure drag, lift, and moment of conductors' model (Figure 5(b)). The data acquisition system is PXI system. The angle and velocity control are realized by the corresponding industrial

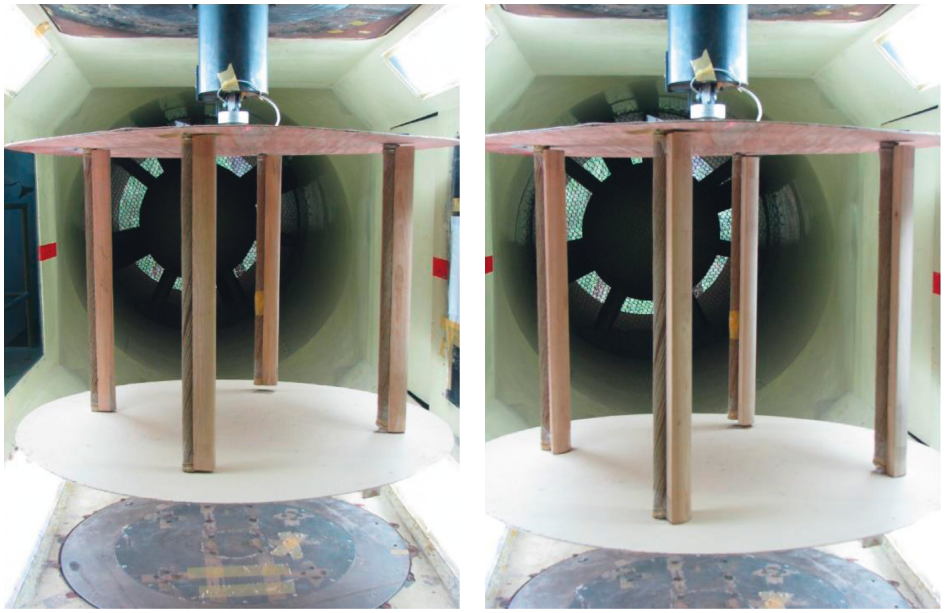

(a) (b)

Figure 3: Photos of iced 4-bundle conductors in wind tunnel: (a) crescent-shape iced conductors and (b) sector-shape iced conductors.

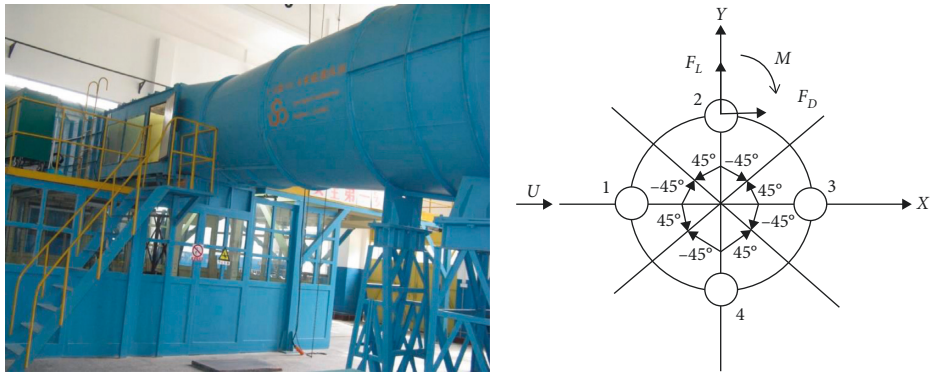

(a) (b)

Figure 4: Support device for test conductor model: (a) wind tunnel and (b) 2D schematic diagram.

Table 1: Symbols and abbreviations.

Symbols	Items	Unit
F_D	Drag	N
F_L	Lift	N
Mz	Moment	Nm
C_d	Drag coefficients	
C_L	Lift coefficients	
C_m	Moment coefficients	
U	Wind velocity	m/s
α	Wind attack angle	°

control computer system. Communication between devices is transmitted by network communication. The parameters of scale and precision of balance TG0151 is shown in Table 2.

The width of the wind tunnel (w_w) is 1400 mm. According to Figures 2 and 3, the width of single bare conductor (w_{con}) is 27.6 mm. For crescent-shape iced conductors, the minimum blockage occurs under the wind attack angle of 0° with single conductor and maximum blockage occurs under the wind attack angle of ±45° with two conductors. However, for sector-shape iced conductor, the minimum blockage occurs under the wind attack angle of ±45° with single conductor and maximum blockage occurs under the wind attack angle of 0° with two conductors. Photos of iced 4-bundle conductors in wind tunnel are shown in Figure 3.

Meanwhile, the minimum blockage and maximum blockage are listed in Table 3; it can be seen that the blockages of iced conductors are different under different wind attack angles and locations. Only few blockages are

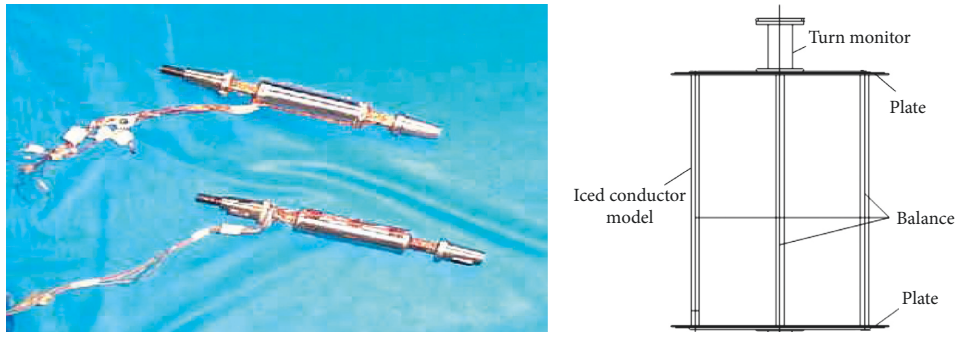

Figure 5: Balance and test device: (a) TG0151 balance; (b) testing device.

Table 2: Scale and precision of TG0151 balance.

Items	Y	M_Z	X	M_X	Z	M_Y
Design load (N, Nm)	60	8	20	1	60	8
Static calibration (%)	0.3	0.3	0.5	0.3	0.3	0.3
Error (%)	0.9	0.9	1.5	0.9	0.9	0.9

Table 3: Minimum and maximum blockage.

		Ice shape				
		Crescent			Sector	
Ice thickness (mm)		14.5	24	33	21.5	30
Blockage (%)	Minimum	3.94	3.94	3.94	3.01	4.06
	Maximum	4.25	5.21	6.12	8.73	10.83

more than 5%. In order to compare, in this test, the data are set to be conservative. All the aerodynamic coefficients have not been corrected. Although it may have some influences on the calculation of aerodynamic coefficients, it does not affect the main conclusions.

3. Unsteady Aerodynamic Coefficients of Iced 4-Bundle Conductors

Compared with the aerodynamic coefficients of single conductor, owing to the wake flow induced by the windward subconductors, the aerodynamic coefficients of the subconductors located in leeward side are significantly different with each other. The definition about the drag, lift, and torsional moment coefficients of the iced subconductor is shown in the references [16, 20, 23]. In the test, the aerodynamic loads exerted on each subconductor are measured by balance; the unsteady drag coefficient C_D, lift coefficient C_L, and moment coefficient C_M of each subconductor can be calculated with equation (1), where ρ is the density of the air at room temperature, L is the length of the conductor, and U is the wind velocity. It is known that iced conductor motion usually occurs in a certain wind velocity range from 4 m/s to 20 m/s (Section 2.2); the wind velocity is set to be 10 m/s, 12 m/s, 14 m/s, and 18 m/s during wind tunnel test.

$$C_L = \frac{F_L}{(1/2)\rho U^2 L d},$$
$$C_D = \frac{F_D}{(1/2)\rho U^2 L d}, \quad (1)$$
$$C_M = \frac{M}{(1/2)\rho U^2 L d^2}.$$

According to Table 1, F_D, F_L, and M are the drag, lift, and torsional moment located on the iced subconductors, respectively. They depend on the parameters such as cross-sectional geometry characteristics of the iced subconductors, the location, and wind attack angle in certain time. The unsteady aerodynamic forces of the subconductors are different between each other. The unsteady inertial force of the model was measured before the dynamic test.

In order to ensure the accuracy of galloping traces measured in the test, the data are the average of eight cycles. The main purpose of average galloping trace is to ensure the stability of the data when the galloping state taken in the test result is stable.

3.1. Influence of Torsional Motion Frequencies on Unsteady Aerodynamic Coefficients. At the wind attack angles −45° to 45°, the unsteady aerodynamic coefficients of iced 4-bundle conductors under typical torsional frequencies (0.1 Hz, 0.2 Hz, and 0.33 Hz, Section 2.2) are shown in Figure 6. Comparing the unsteady and steady (0 Hz, [16]) drag coefficients of crescent-shape iced 4-bundle conductors, the trend of the unsteady and steady aerodynamic characteristics curve of the crescent-shape ice is similar.

For the crescent-shape ice, the unsteady drag coefficient C_D, curve of subconductor 1, presents an approximate parabolic loop from −45° to 45° with a middle low and two sides high (Figure 6(a)), which is different with steady coefficients [16]. Because of the separation of flow and the shedding of vortex at typical wind attack angles, the aerodynamic forces loaded on the conductor surface lag the conductor motion, which makes the aerodynamic force show hysteresis effect with the variety of unsteady wind attack angle. This phenomenon is named "aerodynamic hysteresis effect." Meanwhile, most curves of steady

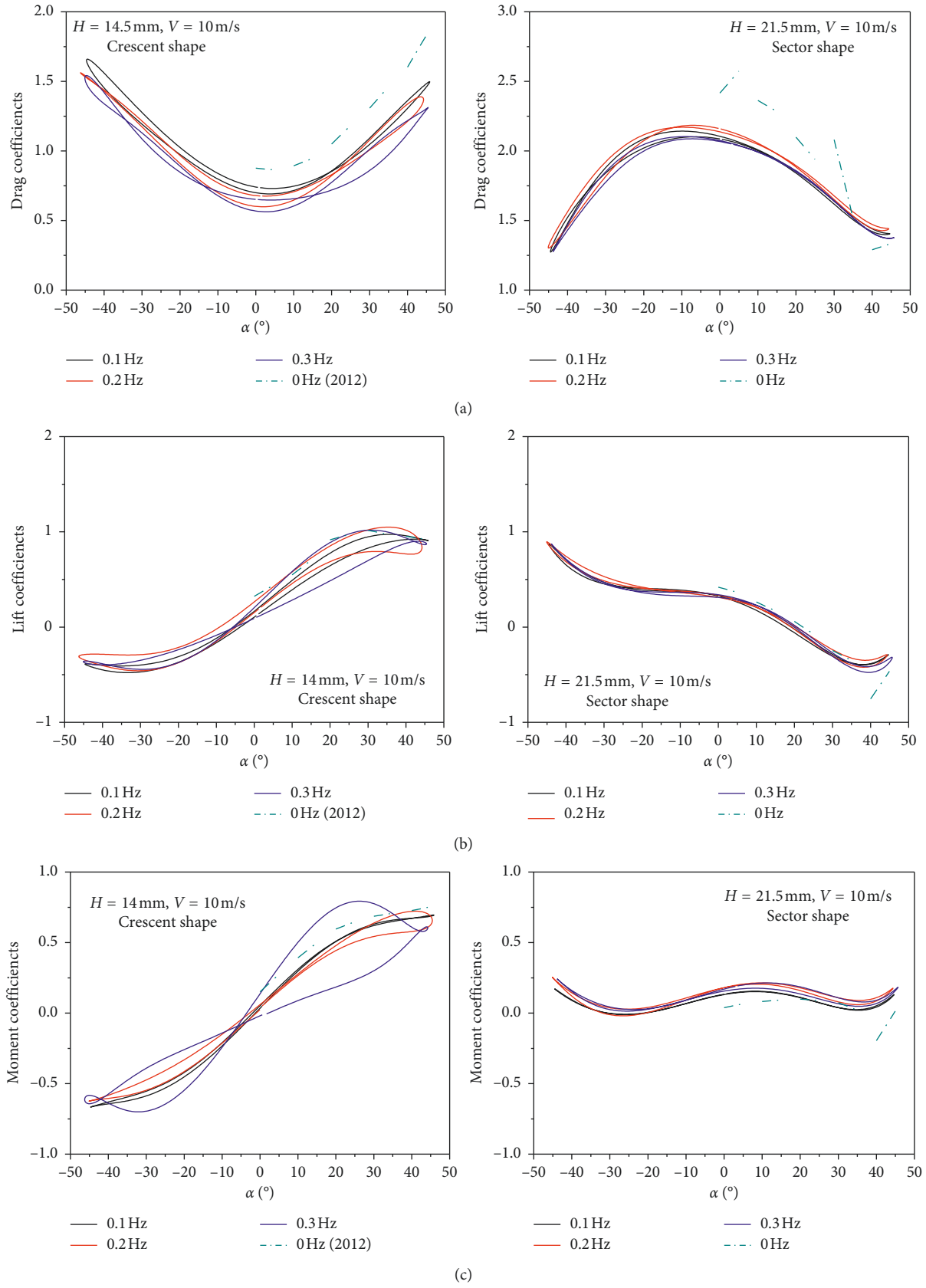

Figure 6: The unsteady aerodynamic coefficients of crescent-shape and sector-shape iced subconductor 1 under different frequencies: (a) drag coefficients; (b) lift coefficients; (c) moment coefficients.

aerodynamic coefficients are within the loop of the unsteady aerodynamic coefficients curve. As can be seen from Figure 5(a), the higher the frequency is, the larger the envelope of the unsteady C_D curve is.

The unsteady lift coefficients C_L and unsteady moment coefficients C_M of iced 4-bundle conductors varying with the wind attack angles from −45° to 45° under different torsional frequencies are shown in Figures 6(b) and 6(c). Similarly, the steady lift and moment coefficients are nearly within the envelope of the unsteady coefficients curve. Similar with the unsteady C_D curve, as shown in Figures 6(b) and 6(c), the higher the frequency is, the larger the envelope of the unsteady lift and moment coefficients curve is.

For the sector-shape ice, the unsteady C_D curve of subconductor 1 presents an approximate parabolic loop from −45° to 45° with a middle high and two sides low (Figure 6(a)). Similar with unsteady C_D curve of crescent-shape iced subconductor 1, the unsteady C_D curve of subconductor 1 shows the loop in the wind attack angle of −45° to 45°, which is different with steady aerodynamic coefficients. The unsteady C_L curve of the sector-shape iced 4-bundle conductors varies from positive to negative, and there are two negative peaks on each side of the curve (Figure 6(b)). The unsteady C_M curves present W-shape loop (Figure 6(c)). The unsteady C_L and C_M of sector-shape iced subconductor suddenly drop under the wind attack angle of 35° because of the ice shape.

3.2. Unsteady Aerodynamic Coefficients of Different Subconductors. Compared with single conductor, the aerodynamic coefficients of the subconductors located in leeward side are obviously different which is attributed to the wake flow induced by the windward subconductors. For crescent-shape ice, the unsteady C_D curve of subconductor 1 shows *V*-shape loop (Figure 7(a), left). The unsteady C_D curve of subconductor 3 shows *M*-shape loop. The unsteady C_D curve of subconductor 2 and 4 shows *S*-shape loop. Meanwhile, it shows that the unsteady C_D curve of the subconductors 2 and 4 are substantially antisymmetric at the wind attack angles ranging from −45° to 45°.

At the wind attack angle of −45°, the subconductors 3 and 4 are in downstream of subconductors 2 and 1, which can result in significant dropping at this wind attack angle. Similarly, at wind attack angle of 45°, the subconductors 3 and 2 are in downstream of subconductors 4 and 1, which also results in significant dropping of C_D at the wind attack angle of 45°, referring to Figure 4(b). Meanwhile, the subconductor 1 is always located in the windward side from attack angle −45° to 45°. These results note the unsteady aerodynamic characteristics of bundle conductors are obviously affected by the wake disturbance of air flow around bundle conductors.

For the sector-shape ice (Figure 7(a), right), the unsteady C_D curve of subconductor 1 presents an approximate inverse parabolic loop with higher in middle and lower at two sides. The unsteady C_D curve of subconductor 2 presents the loop shape with higher value around wind attack angle of −15° and lower at two sides. The unsteady C_D curve of subconductor 3 shows an approximate *M*-shape loop, which is caused by the ice shape. The unsteady C_D curve of subconductor 4 shows the loop with higher value around wind attack angle of 15° and lower at two sides. Compared with unsteady aerodynamic coefficients of crescent-shape iced 4-bundle conductors, it is obvious that the aerodynamic forces of the crescent-shape iced 4-bundle conductors changing with the wind attack angles are different from that of the sector-shape ice.

At the wind attack angles −45° to 45°, the unsteady C_L of two types of ice-shape covered subconductors is substantially antisymmetric, which is shown in Figure 6(b). The unsteady C_L curves of crescent-shape iced conductors show *S*-shape loop with higher on the right side and lower on the left side (Figure 7(b), left). However, the unsteady C_L curves of sector-shape iced conductors show *wave*-shape loop with higher on the left side and lower on the right side (Figure 7(b), right). It shows that wake disturbance has evident effects on lift coefficients of leeward subconductors in Figure 7(b).

In Figure 7(c), at the wind attack angles −45° to 45°, it can be seen that the unsteady C_M of the subconductor is also asymmetric, and the variation tendency is similar as the lift coefficients. The unsteady C_M curves of crescent-shape iced conductors show *S*-shape loop with left side high and right side low (Figure 7(c), left). However, the unsteady C_M curves of sector-shape iced conductors show *wave*-shape loop with higher on the left side and lower on the right side (Figure 7(c), right). Compared with unsteady C_D (Figure 7(a)), it explains that the wake flow has no obvious effect on the moment coefficients of leeward subconductors, which is shown in Figure 7(c).

It is obvious that the unsteady aerodynamic coefficients of the sector-shape iced 4-bundle conductors varying with the wind attack angles are different from that of the crescent-shape ice (Figures 6 and 7). The variation of the aerodynamic coefficients varying with wind angle of attack of these two types of shape of iced subconductors is totally different. The influence of ice shape on aerodynamic characteristics of iced bundle conductors is significant.

3.3. Influence of Wind Velocity on Unsteady Aerodynamic Coefficients. In order to research the influence of wind velocity on unsteady aerodynamic coefficients, the unsteady aerodynamic parameters of crescent-shape and sector-shape iced subconductor 1 under typical wind velocity (10 m/s, 12 m/s, 14 m/s, and 18 m/s) are measured. It can be seen in Figure 8(a) that the unsteady C_D of crescent-shape and sector-shape iced subconductor 1 slightly decreases when wind velocity increases. The unsteady C_L and C_M of crescent-shape and sector-shape iced subconductor 1 are almost the same under these four different wind velocities (Figures 8(b) and 8(c)).

In the wind test condition, the Reynolds number (Re) is an important parameter of the type of flow characteristics. The range corresponds to the range including the so-called critical range, where the characteristics of lift and moment indicate a drastic transition.

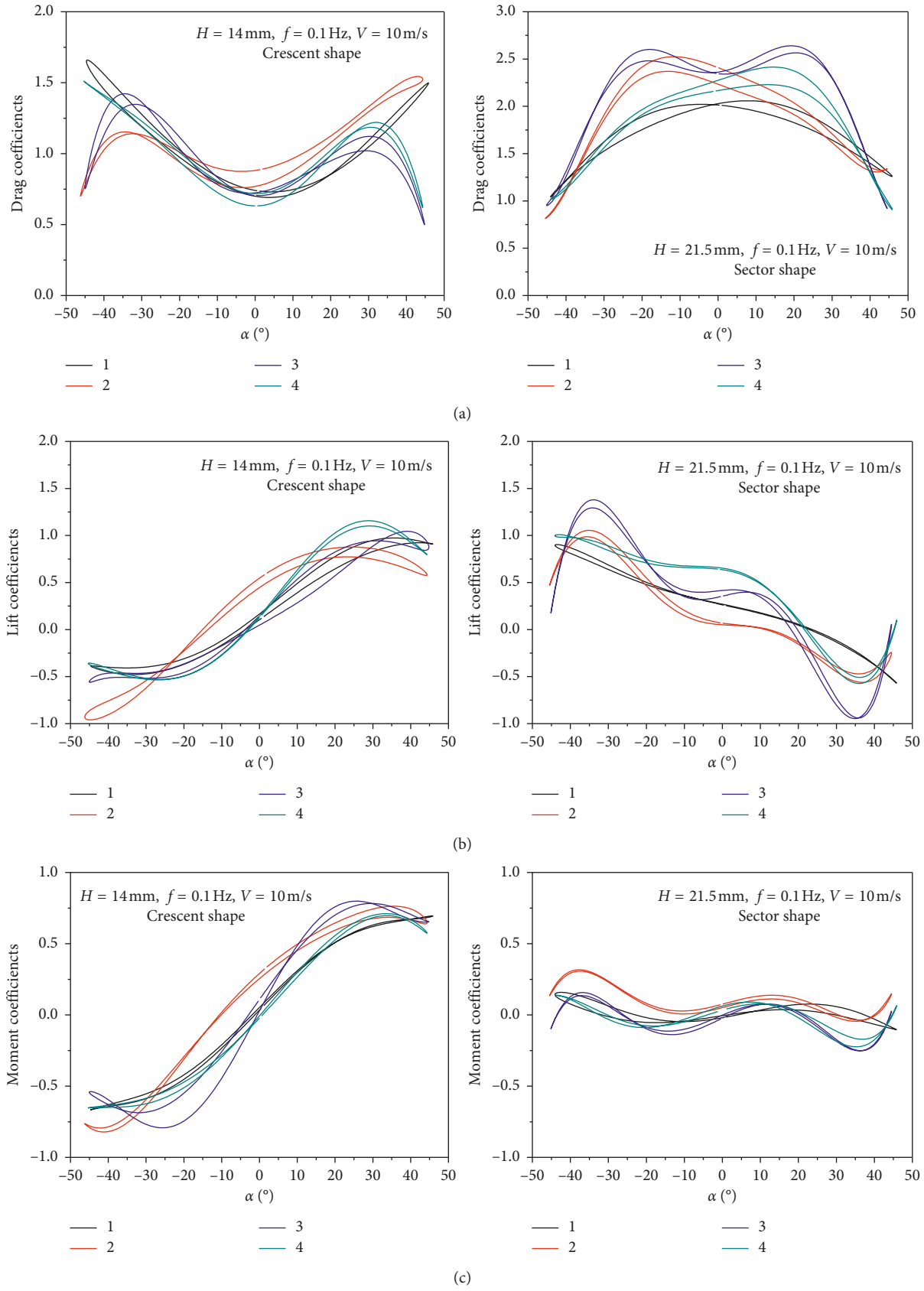

Figure 7: The unsteady aerodynamic coefficients of each iced subconductors: (a) drag coefficients; (b) lift coefficients; (c) moment coefficients.

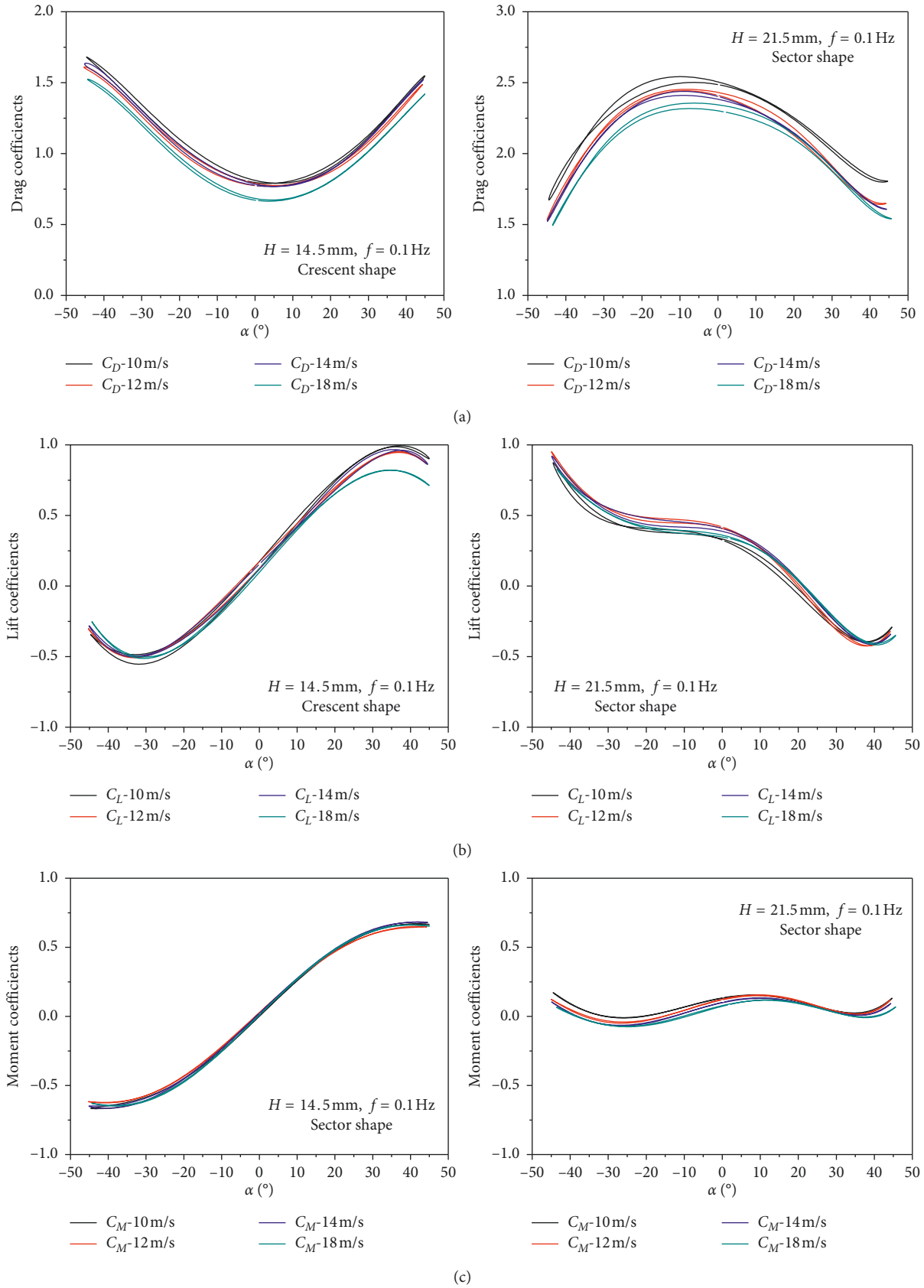

Figure 8: The unsteady aerodynamic coefficients of iced subconductor 1 under different wind velocities: (a) drag coefficients; (b) lift coefficients; (c) moment coefficients.

$$\mathrm{Re} = \frac{\rho U L_0}{\mu} = \frac{U L_0}{\nu}, \quad (2)$$

where μ is the viscosity of the air. $\nu = \rho/\mu$ is the kinematic viscosity. L_0 is simplified as the diameter of the subconductor and the ice thickness. The kinematic viscosity of the air is 1.7894×10^{-5}. These wind velocities are ranging from 10 m/s to 18 m/s; the corresponding Re is around 2.0×10^4–5.0×10^4 in this condition. The results indicate that in the range of magnitude (10^4) of Re, the unsteady aerodynamic coefficients are almost not changing with Re.

3.4. Influence of Ice Thickness on Unsteady Aerodynamic Coefficients. In order to research the effects of ice thickness on unsteady aerodynamic behaviors, the unsteady aerodynamic coefficients of crescent-shape iced (14.5 mm, 24 mm, and 33 mm) and sector-shape iced (14.5 mm and 30 mm) subconductor 1 are measured and analyzed. The unsteady aerodynamic coefficients of subconductor 1 with different ice thicknesses are shown in Figure 9.

At the wind attack angles −45° to 45°, the unsteady C_D of crescent-shape iced subconductor 1 with different ice thicknesses (14.5 mm, 24 mm, and 33 mm) is shown in Figure 9(a) (left). When the ice thickness increases to thicker ice thickness (i.e., 24 mm or 33 mm), it shows that the unsteady C_D of subconductor 1 suddenly drops at the wind attack angle of 0°; this is mainly because the outline of the conductor is changed suddenly around the wind attack angle of 0° according to the incoming flow, which means the wind attack angle of 0° is a critical angle. It can be seen that at the wind attack angle (−45° to 45°), the unsteady C_D of the windward subconductor 1 is substantially symmetrical. Meanwhile, when the wind attack angle is around −45°~−15° and 15°~45°, the unsteady C_D of the windward crescent-shape iced subconductor 1 decreases with the increase of the ice thickness.

The unsteady C_D of sector-shape iced subconductor 1 with different ice thicknesses (21.5 mm and 33 mm) under wind attack angle of −45°~45° is shown in Figure 9(a) (right). It shows that at these wind attack angles (−45° to 45°), the unsteady C_D of the sector-shape iced subconductor 1 significantly decreases with the increasing of the ice thickness.

The unsteady C_L of crescent-shape iced subconductor 1 with different ice thicknesses (14.5 mm, 24 mm, and 33 mm) is shown in Figure 9(b) (left). The unsteady C_L of crescent-shape iced subconductor 1 increases with the increasing of the ice thickness at these wind attack angles (−45° to 45°), particularly around the wind attack angle of ±20°. The reason for that phenomenon is that the unsteady C_L of crescent-shape iced subconductors rapidly increases with the increase of the ice thickness.

The unsteady C_L of sector-shape iced subconductor 1 with different ice thicknesses (21.5 mm and 33 mm) is shown in Figure 9(b) (right). At the range of the wind attack angles different with the unsteady C_L of crescent-shape subconductor, sector-shape iced subconductor 1 slowly increases with the increase of the ice thickness. Because of the wind attack angle ranging from −45° to 45°, the surface outline of the conductor changes slowly according to the incoming flow.

At the wind attack angles −45° to 45°, the unsteady C_M of subconductor 1 with different ice thicknesses is shown in Figure 9(c). The profiles of unsteady C_M of two types of ice-shape covered subconductor 1 are approximately antisymmetric, the same as the unsteady C_L at the wind attack angles (−45° to 45°). There is a great influence of ice thickness on the unsteady C_M of the crescent-shape iced subconductor 1; the absolute values of the unsteady C_M increase with the increase of the ice thickness. The increasing trend of the coefficients curve increases much obviously than that of the increasing of ice thickness.

However, different from crescent-shape iced subconductors, at the range of wind attack angles, the unsteady C_M of sector-shape iced subconductor 1 increases slowly with the increase of the ice thickness (Figure 9(c), right). Because at the wind attack angles (−45° to 45°), the surface outline of the sector-shape iced conductor changes slowly. The absolute value of unsteady C_M of sector-shape iced subconductor 1 increases slightly around the wind attack angle of ±30°.

4. Conclusions

In the study, wind tunnel tests are used to acquire the unsteady aerodynamic coefficients of iced 4-bundle conductors. These influences of several key factors on those unsteady aerodynamic characteristics of iced 4-bundle conductors at varying wind attack angles are studied in detail. According to the results, the following conclusions can be drawn:

(1) The unsteady aerodynamic behaviors of individual subconductors are obviously different due to the surrounding flow interference. The unsteady drag coefficients of iced 4-bundle conductors are obviously affected by the wake flow, but the unsteady lift and moment coefficients are less affected.

(2) Different from steady aerodynamic coefficients, the unsteady aerodynamic coefficient curve of iced conductor is loop shape.

(3) Because of the different cross section of iced 4-bundle conductors, the unsteady aerodynamic characteristics of crescent-shape and sector-shape iced 4-bundle conductors are totally different.

(4) Within the given range of wind velocity, the wind velocity has nearly no influence on the lift and moment coefficients but has a less influence on the drag coefficients.

(5) The unsteady drag, lift, and moment coefficients of these iced 4-bundle conductors increase with the increase of the ice thickness at the whole wind attack angles.

These test results provide some useful references and theoretical basis for the study of conductor motion in cold regions.

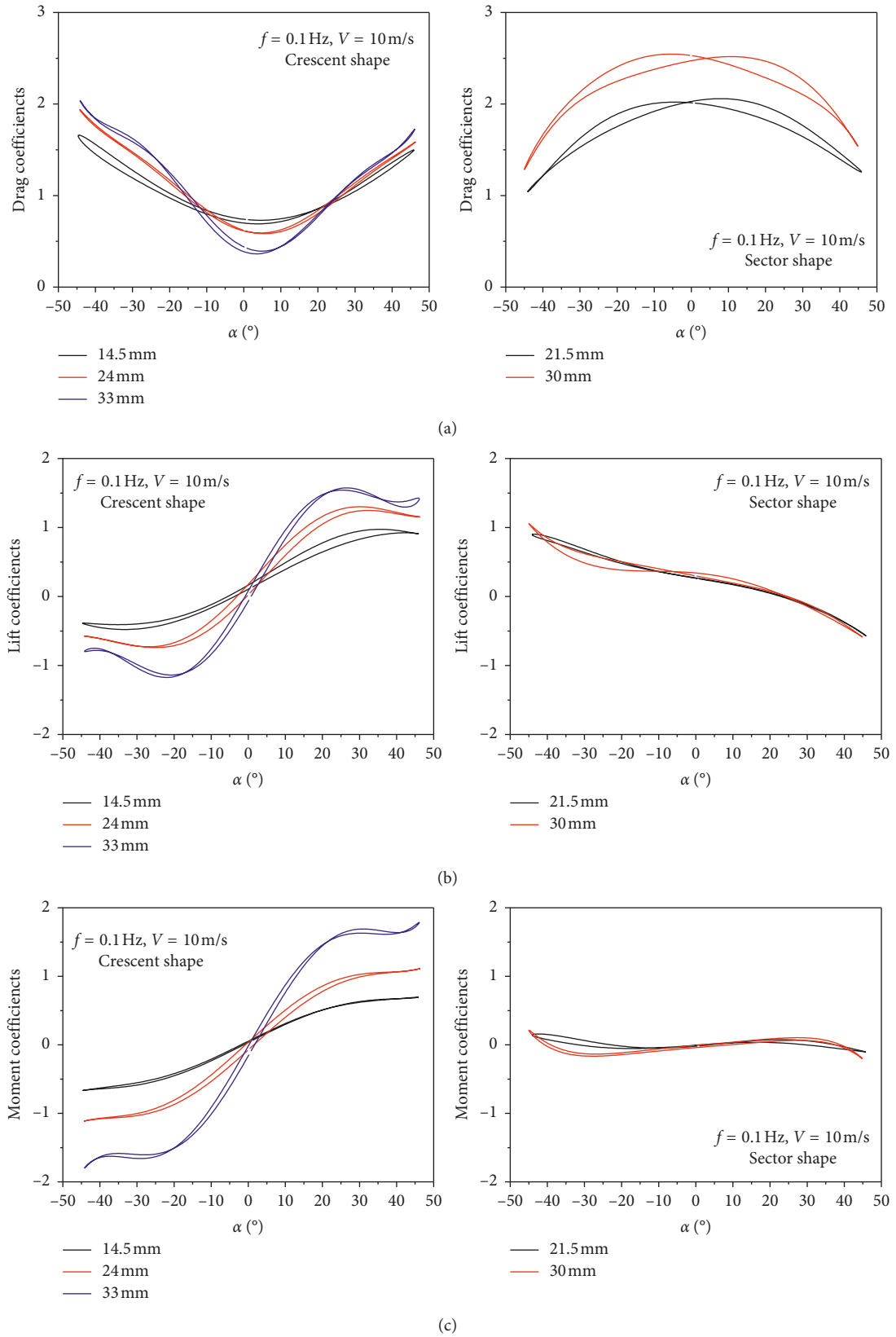

Figure 9: The unsteady aerodynamic coefficients of sector-shape iced subconductor 1 under different ice thickness: (a) drag coefficients; (b) lift coefficients; (c) moment coefficients.

Data Availability

The data used to support the findings of this study are available from the corresponding author upon request.

Conflicts of Interest

The authors declare that there are no conflicts of interest regarding the publication of this paper.

Authors' Contributions

Hanjie Huang designed the test model and finished the aerodynamic coefficients measurement of 4-bundle conductors; Cai Mengqi designed the research plan; Mengqi Cai and Linshu Zhou participated in the investigation of the aerodynamic coefficients obtained in the wind tunnel test; and Hang Lei participated in data analysis. All authors gave final approval for publication.

Acknowledgments

This work was financially supported by the National Natural Science Foundation of China (51507106), Science Foundation of Henan (SGTYHT/15-JS-194), Electric Power Research Institute, and China State Scholarship Fund (201708515019). Mengqi Cai wishes to thank Prof. Xi Chen for his useful advices on this research during the visit to Columbia University as research scholar.

References

[1] K. Savadjiev and M. Farzaneh, "Probabilistic model of combined wind and ice loads on overhead power line conductors," *Canadian Journal of Civil Engineering*, vol. 30, no. 4, pp. 704–710, 2003.

[2] P. Fu and M. Farzaneh, "Simulation of the ice accretion process on a transmission line cable with differential twisting," *Canadian Journal of Civil Engineering*, vol. 34, pp. 704–710, 2007.

[3] Electric Power Research Institute, *Transmission Line Reference Book: Wind Induced Conductor Motion*, Electric Power Research Institute, Palo Alto, CA, USA, 2009.

[4] J. P. D. Hartog, "Transmission line vibration due to sleet," *Transactions of the American Institute of Electrical Engineers*, vol. 51, no. 4, pp. 1074–1076, 1932.

[5] J. Wang and J. L. Lilien, "Overhead electrical transmission line galloping: a full multi-span 3-DOF model, some applications and design recommendations," *IEEE Transactions on Power Delivery*, vol. 13, no. 3, pp. 909–916, 1998.

[6] R. L. Wardlaw, K. R. Cooper, R. G. Ko, and J. A. Watts, "Wind tunnel and analytical investigations into the aeroelastic behaviour of bundled conductors," *IEEE Transactions on Power Apparatus and Systems*, vol. 94, no. 2, pp. 642–654, 1975.

[7] M. Shimizu, T. Ishihara, and P. V. Phuc, "A wind tunnel study on aerodynamic characteristics of ice accreted transmission lines," in *Proceedings of the 5th International Colloquium on Bluff Body Aerodynamics and Applications*, Ottawa, Canada, July 2004.

[8] A. Barrero, A. Sanz, and G. Alonso, "Hysteresis in transverse galloping: the role of the inflection points," *Journal of Fluids and Structures*, vol. 25, pp. 1007–1020, 2009.

[9] A. Raeesi, S. Cheng, and D. S.-K. Ting, "Aerodynamic damping of an inclined circular cylinder in unsteady flow and its application to the prediction of dry inclined cable galloping," *Journal of Wind Engineering and Industrial Aerodynamics*, vol. 113, pp. 12–28, 2013.

[10] G. Diana, M. Belloli, S. Giappino et al., "A numerical approach to reproduce subspan oscillations and comparison with experimental data," *IEEE Transactions on Power Delivery*, vol. 29, no. 3, pp. 1311–1317, 2014.

[11] O. Nigol, G. J. Clarke, and D. G. Havard, "Torsional stability of bundle conductors," *IEEE Transactions on Power Apparatus and Systems*, vol. 96, no. 5, pp. 1666–1674, 1977.

[12] O. Nigol and P. Buchan, "Conductor galloping Part I—den Hartog mechanism," *IEEE Transactions on Power Apparatus and Systems*, vol. PAS-100, no. 2, pp. 699–707, 1981.

[13] O. Nigol and P. Buchan, "Conductor galloping-Part II torsional mechanism," *IEEE Transactions on Power Apparatus and Systems*, vol. PAS-100, no. 2, pp. 708–720, 1981.

[14] O. Chabart and J. L. Lilien, "Galloping of electrical lines in wind tunnel facilities," *Journal of Wind Engineering and Industrial Aerodynamics*, vol. 74–76, pp. 967–976, 1998.

[15] R. L. Wardlaw and K. R. Cooper, "A wind tunnel investigation of the steady aerodynamic forces on smooth and stranded twin bundle power conductors for the Aluminum Company of America," Lab Tech Rep. LA-117, NRC, Ottawa, Canada, 1973.

[16] J. Hu, B. Yan, S. Zhou, and H. Zhang, "Numerical investigation on galloping of iced quad bundle conductors," *IEEE Transactions on Power Delivery*, vol. 27, no. 2, pp. 784–792, 2012.

[17] Q. Xie, Q. Sun, Z. Guan, and Y. Zhou, "Wind tunnel test on global drag coefficients of multi-bundled conductors," *Journal of Wind Engineering and Industrial Aerodynamics*, vol. 120, pp. 9–18, 2013.

[18] G. Diana, M. Belloli, S. Giappino et al., "Wind tunnel tests on two cylinders to measure subspan oscillation aerodynamic forces," *IEEE Transactions on Power Delivery*, vol. 29, no. 3, pp. 1273–1283, 2014.

[19] B. Yan, M. Q. Cai, X. Lyu, and L. S. Zhou, "Numerical simulation on wake galloping of quad bundle conductor," *Journal of Vibration and Shock*, vol. 34, no. 1, pp. 182–189, 2015, in Chinese.

[20] B. Yan, X. H. Liu, X. Lv, and L. S. Zhou, "Investigation into galloping characteristics of iced quad bundle conductors," *Journal of Vibration and Control*, vol. 13, pp. 967–986, 2016.

[21] X. M. Li, X. C. Nie, Y. K. Zhu, Y. You, and Z. T. Yan, "Wind tunnel tests on aerodynamic characteristics of ice-coated 4-bundle conductors," *Mathematical Problems in Engineering*, vol. 29, no. 3, pp. 1273–1283, 2017.

[22] W. Lou, J. Lv, M. F. Huang, L. Yang, and D. Yan, "Aerodynamic force characteristics and galloping analysis of iced bundled conductors," *Wind and Structures*, vol. 18, no. 2, pp. 135–154, 2014.

[23] L. Zhou, B. Yan, L. Zhang, and S. Zhou, "Study on galloping behavior of iced eight bundle conductor transmission lines," *Journal of Sound and Vibration*, vol. 362, pp. 85–110, 2016.

[24] M. Cai, B. Yan, X. Lu, and L. S. Zhou, "Numerical simulation of aerodynamic coefficients of iced-quad bundle conductors," *IEEE Transactions on Power Delivery*, vol. 30, no. 4, pp. 1669–1676, 2015.

[25] C. Wu, Bo. Yan, G. Z. Huang, B. Zhang, Z. B. Lv, and Q. Li, "Wake-induced oscillation behaviour of twin bundle conductor transmission lines," *Royal Society Open Science*, vol. 5, no. 6, article 180011, 2018.